coatings

MDPI

Article

Analysis of a Wide Range of Commercial Exterior Wood Coatings

Michael J. Gibbons [1], Saeid Nikafshar [2], Tina Saravi [1], Katie Ohno [3], Sanjeev Chandra [1] and Mojgan Nejad [2,4,*]

[1] Centre for Advanced Coating Technologies, University of Toronto, Toronto, ON M5S 2E4, Canada; Michael.Gibbons@tcd.ie (M.J.G.); Tina.saravi@mail.utoronto.ca (T.S.); chandra@mie.utoronto.ca (S.C.)
[2] Department of Forestry, Michigan State University, East Lansing, MI 48824, USA; nikafsha@msu.edu
[3] Forest Products Laboratory, Madison, WI 53726, USA; katie.m.ohno@usda.gov
[4] Chemical Engineering and Material Science Department, Michigan State University, East Lansing, MI 48824, USA
* Correspondence: nejad@msu.edu; Tel.: +1-517-355-9597

Received: 27 September 2020; Accepted: 19 October 2020; Published: 22 October 2020

Abstract: This study was focused on measuring the properties of twenty-three commercially available coatings formulated for exterior wood applications. The coatings were characterized by measuring their surface tension, solid content, viscosity, pH, and glass transition temperatures (T_g). Additionally, the wetting properties of coating droplets on wood substrates were measured. The contact angle of solvent-based and water-based coatings were characterized on untreated southern yellow pine wood samples using high-resolution image analysis and the Young–Laplace solution. An innovative image processing technique for determining the average diameter of coating droplets on wood was developed, and an iterative method to calculate the average contact angle using the Young–Laplace solution was applied. The water-resistance of the coated wood samples was evaluated during one week of water immersion tests. In general, solvent-based coatings had significantly lower contact angles and water uptake than water-based coatings. Water-based paint samples had the largest average contact angle (81°), and solvent-based transparent penetrating stains had the smallest contact angle (13.9°). A strong correlation was observed between the coating water uptake and their surface tension and solid content.

Keywords: droplet spreading; wood coating; Young–Laplace solution; wettability; water uptake

1. Introduction

Engineered wood products are becoming an essential material in the construction of both residential and commercial buildings. Wood is a complex biopolymer [1–5] that needs to be protected by an effective coating when exposed to solar radiation, water, varying temperatures, and oxygen [5]. Making durable wood coatings is essential in extending the service life of coated products and reducing maintenance [5]. The performance of a coating in exterior applications depends on many factors such as wood species and their physical properties, coating types and properties, application procedures, and exposure conditions [6]. In addition to accentuating the aesthetics of a natural substrate, an exterior coating is designed to protect the wood from moisture, ultraviolet (UV) radiation, and mildew discoloration [7,8].

Among these factors, UV degradation and moisture effects are the most influential factors on the performance of coated wood [6]. Photo-oxidation occurs rapidly when exposed wood in the presence of oxygen interacts with ultraviolet and visible light [9]. Photo-oxidation primarily affects the lignin component of wood and induces surface property modification such as discoloration, increased water sensitivity followed by hydrolysis, checking, and cracking [10,11]. These processes

detrimentally deteriorate the wood's appearance and structural properties. Changes in the moisture content of wood result in the swelling and shrinking of the material, leading to stresses and the checking of the wood. If the water stays in the wood, it will create suitable conditions for the growth of decay fungi inside the wood [6]. The repeated freezing and thawing of liquid water in wood cells results in additional stresses; small cracks will develop, and these later expand to checks if the wood remains exposed to outdoor conditions [12,13]. Wind and wind-driven particles erode the exposed surface, contributing to uneven wear in the earlywood and latewood. Unlike weathering, decay fungi and insects can ultimately deteriorate the wood and cause severe structural damage. Wood should be coated in a protective finish to inhibit the effect of weathering in outdoor exposure [14].

The application of surface coatings on wood is an excellent method of protecting and maintaining the appearance and performance of wooden structures [7]. Coatings can reduce the water uptake, UV-degradation, and checking of wood, which prolongs the service life of wooden products [6]. Coatings generally consist of four main components: (1) resins or binders, (2) pigments, (3) solvents, and (4) other additives. Different coating formulations may not have all these four main components [6]. High-performance coatings formulated for wood should be able to provide excellent water repellency but also have good water vapor permeability to allow moisture to escape from the surface of the wood [15,16]. The degree of UV protection that any coating provides primarily depends on the pigment density of the formulation [17,18]. Transparent coatings on exterior wood require frequent reapplication (every one-to-two years) to ensure continued protection [6]. This requirement makes wood a high-maintenance product when compared to other building materials. Increasing the lifespan of coatings would reduce the required maintenance and encourage the more extensive use of wood as a building material.

Coatings have very complex formulations, and their interactions with a natural material like wood makes predictions of their service life and performance challenging [19]. Coating performance and lifecycle are dependent on factors such as grain characteristics, surface texture, heartwood/sapwood ratio, knots, extractives, moisture content, and density [20–22]. One of the most critical factors in determining coating performance is the wetting characteristics of the coating and wood constituents. The durability of any coating is strongly dependent on the adhesion of the protective coating layer to the substrate [23]. The characterization of the wetting behavior of a coating is essential in defining coating adhesion strength. The magnitude of the contact angle of a coating droplet on a substrate is widely used as a measure of the wettability of a coating-surface combination [6,24].

A lower contact angle indicates better wetting and subsequent greater bond strength between a coating and substrate. In general, to have excellent wetting, a coating should have a significantly lower surface tension compared to the surface energy of its substrate [25]. The contact angle of early and latewood should be considered, as the contact angle is typically much higher on latewood than earlywood [26]. A traditional method of characterizing the contact angle of a solid–liquid interface is conducted using a side-view method, which is shown in Figure 1. In this configuration, an optical camera is placed parallel to the substrate being investigated [27–30].

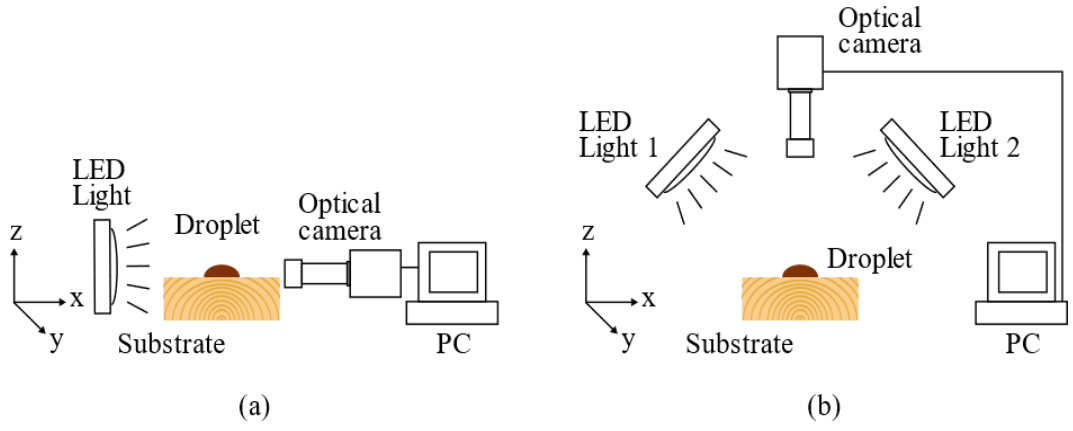

Figure 1. Experimental set-up schematic: (**a**) Side-view approach and (**b**) top–down approach.

The contact angle, in this approach, is determined by drawing a line from the contact line (solid-liquid-gas interface) tangential to the liquid-gas interface. An example of this is illustrated by the red lines drawn in Figure 2a,b. The angle of these lines relative to the substrate is the contact angle. This method is not suitable for use with natural substrates, as it relies on the assumption of an axisymmetric droplet. This is not correct for a coating droplet on wood due to the substrate's anisotropic non-smooth nature, and it can be inaccurate for low contact angles.

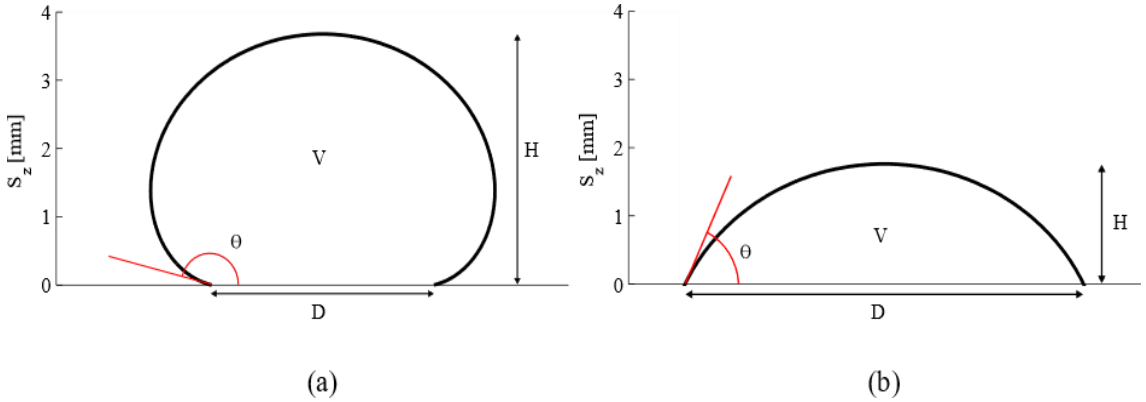

Figure 2. Droplet schematic and parameters: (**a**) hydrophobic droplet and (**b**) hydrophilic droplet.

Coating wetting through contact angle characterization on wood [24,31–33] and other surfaces [34,35] has been previously studied. Kazayawoko et al. [24] outlined a top-down approach to determine a coating droplet contact angle on wood, as shown in Figure 1b. In this approach, an optical camera is placed perpendicular to the substrate, and the average diameter of the droplet is determined. By knowing the droplet volume, surface tension, and density, it is possible to iteratively solve the Young–Laplace equation to converge on an average contact angle solution. Kazayawoko et al. [24] detected the droplet base diameter on wood by manually placing 15–20 points on the perimeter of each droplet. This technique is time-consuming, requires human input, which has an associated error, and is unable to analyze highly irregular shapes. Given current technology and image processing techniques that are now widely available, it is possible to automate this process, thus making it possible to efficiently characterize an extensive range of coating-substrate combinations.

Meijer et al. [32] calculated the Lifshitz-van der Waals, acid-base, and total surface free energies of various wood species from contact angle measurements. Three distinct methods of contact angle measurement were employed: capillary rise based on the Washburn equation, dynamic contact angle measurements according to the Wilhelmy-plate principle, and sessile drop measurements along and across the grain of the wood. The impact of substrate chemical heterogeneity, surface roughness, and the adsorption of the test solvent was discussed. Shi and Gardner [31] explored adhesive wettability on wood. They developed a wetting model to describe the dynamic contact angle during the adhesive wetting process on southern pine and Douglas-fir. Baptista et al. [33] investigated contact angle characterization utilizing three cameras that were positioned orthogonally on anisotropic substrates such as wood. They assumed that the droplet shape could be approximated by a spherical or ellipsoidal cap and required no fluid properties. The authors noted that their approach was not able to accurately characterize droplets with non-elliptical shapes.

Erbil et al. [34] used images captured from a dual camera orientation (top-down and side-view) to study the evaporation rate of water droplets on poly(methyl methacrylate). The ellipsoidal cap droplet profile was mathematically derived from the base radius, droplet height, and contact angle. Mchale et al. [35] examined the impact of drop flattening and substrate surface heterogeneity on the cross-sectional and planar shapes of droplets on solid surfaces. They employed a dual-camera system to capture views from two orthogonal points of view.

This paper measured the properties of thirteen water-based and ten solvent-based coatings (some of which are shown in Figure 3) on southern yellow pine wood samples. An innovative image

processing technique for coating droplets on wood is presented and discussed regarding the determination of the average droplet diameter and the iterative method of calculating the average contact angle using the top-down approach and the Young–Laplace solution. Additionally, the ability of each coating on reducing water uptake and their water permeability was measured when applied on small cross-laminated timber (CLT) wood samples. The coated wood samples were submerged into water, and their moisture contents were measured at different intervals for up to one-week of submersion in water and then one week of airdrying.

Figure 3. Some of the commercial coatings used in this study.

2. Materials and Methods

2.1. Wood Properties

Flat-grained southern yellow pine wood samples were cut from 6 different boards measuring 2 cm × 12 cm × 30 cm with 8–10 average annual rings. The wood samples were conditioned in the lab at about 65% R.H. and 21 °C for three months before use. A small piece from the middle section of each board was cut to measure its moisture content. The remaining boards were maintained in sealed enclosures to ensure that their moisture contents would not change before being used for contact angle measurements. The wood samples were sanded with 120 grit sandpaper and wiped clean before measuring the contact angle of the coating. The moisture content of a subset of wood samples was analyzed by weighing the wood samples before and after placing them in a digital oven at 105 °C for one hour or until the weight was constant. The moisture content percentage was calculated by subtracting the mass of the oven-dry weight of wood from the initial weight, divided by oven-dry mass times 100.

2.2. Coating Properties

Twenty-three commercially available coatings, thirteen of which were water-based and ten of which solvent-based, were purchased and characterized during this study. The contact angle of all coatings was investigated on flat-grained southern yellow pine wood. Each coating was tested on a minimum of three different boards on both early and latewood cases. The coatings were separated into five categories depending on their base (water or solvent) and their opacity (transparent, semi-transparent, and paint): T.S. (transparent stain, solvent-based), S.S. (semi-transparent stain, solvent-based), T.W. (transparent stain, water-based), S.W. (semi-transparent stain, water-based), and P.W. (paint, water-based). All tests were conducted at room temperature, and average liquid densities of 1100 kg/m^3 and 850 kg/m^3 were used for the water and solvent-based coatings, respectively, in all calculations.

To rigorously investigate the experimental wetting data, several fundamental coating properties were characterized. These coating properties are listed in Table 1. The solid content of coatings was determined according to ASTM D2369 [36]. Briefly, about 3 mL of each coating (5 replicates) were

placed in an aluminum pan and heated in an oven at 110 °C for one hour. The volatile organic compounds of each coating were calculated based on the difference in the mass of the coatings. A Brookfield DV2T Viscometer (Middleboro, MA, USA) was used to measure the viscosity of different coatings at room temperature. The pH of each coating was determined using a Mettler Toledo SevenCompact pH/ion meter S220 (Columbus, OH, USA) based on US EPA Method 9045D. The surface tension of each sample was measured using a Sigma 70 Tensiometer (Phoenix, AZ, USA) using the Wilhelmy plate method (22 mm × 50 mm × 0.15 mm) at a speed of 10 mm/min and a wetting depth of 6 mm, with an average of 10 readings for each sample. The glass transition temperatures of the coatings were measured using a Q2000 differential scanning calorimeter (DSC) (New Castle, DE, USA) and following ASTM D3418 procedure [37]. Briefly, about 6–8 mg of each coating sample were placed in a Tzero aluminum pan with a custom heat/cool/heat cycle from −60 to 120 °C with a temperature ramp of 10 °C/min under nitrogen purge of 50 mL/min. A second heating curve was used to calculate the T_g.

2.3. Experimental Apparatus and Data Acquisition

A schematic and a model of the experimental apparatus are shown in Figures 1b and 4, respectively. In this study, the top–down configuration for determining the droplet contact angle was implemented.

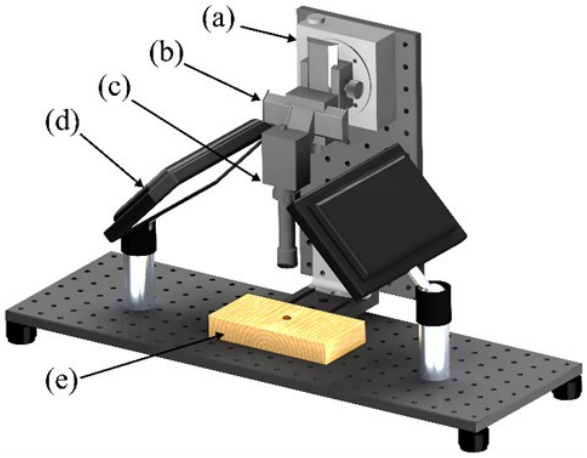

Figure 4. Experimental facility: (**a**) rotation stage, (**b**) *xz*-axis macro positioning stage, (**c**) CCD camera, (**d**) LED light panel, and (**e**) wood substrate.

2.4. Droplet Imaging System

The droplet imaging system consisted of a CCD camera (Point Grey, sensor: Sony IMX250, sensor size: 2/3″; pixels: 2448 × 2048; pixel depth: 12 bit; P/N: GS3-U3-51S5M-C) and a telecentric lens (Edmund Optics, magnification: 0.8×; working distance: 65 mm; depth of field: 1.2 mm; P/N: 63-742) (Figure 4c). The optical camera was vertically mounted to a 2-axis (*x* and *z*) macro positioning system (Cameron, P/N: 4638) (Figure 4b) that was connected to a rotation stage (Newport, P/N: 472) (Figure 4a). The wood sample was placed directly below the optical camera, perpendicular to the wood surface during testing. The wood substrate was illuminated by two LED panel arrays (IKAN, 7″ × 4″, P/N: PL74) (Figure 4d) that were mounted to an aluminum baseplate (Edmund Optics, P/N: 03-639).

2.5. Contact Angle Measurement

Experiments were conducted in ambient surroundings at atmospheric pressure for a typical relative humidity of 31%. During testing, the wood samples were positioned directly below the optical camera (Figure 4e). A syringe pump (NE-1000, New Era, Buffalo, NY, USA), a 100 µL gastight syringe (Hamilton 1710, 81022, Hamilton, Reno, NV, USA), and 100 µm inner diameter FEP tubing (1474-20, Wilmington, DE, USA) were used to dispense the droplet onto the wood surface. A coating droplet of varied volume (3–10 µL) was dispensed at 60 µL/min onto the natural substrate for each

test point. The volume dispensed depended on the expected maximum spreading diameter of the drop. At the start of each test, the optical camera and syringe pump were triggered simultaneously. Images were acquired at 1 s intervals over a 10 min period.

2.6. Water Immersion Test

For the water immersion test, small samples of commercially prepared cross-laminated timber (CLT) were used measuring 106 mm × 50 mm × 10.8 mm. The CLT, Douglas-fir wood samples were sanded with 120 grit sandpaper and cleaned before the application of coatings; 2.36 g of water-based coatings and 1.82 g of solvent-based coatings were applied to the CLT samples using a foam brush to achieve a consistent wet film thickness for all coating (152.4 μm/6 mils coating thickness). The amount of coatings needed was calculated based on the surface area of the wood sample and the average density of the water-based (1.1 g/m^3) and solvent-based (0.85 g/m^3) coatings. After one week of air drying (Figure 5), samples were immersed in DI water (five replicates for each coating; the only three replicates that could fit on the surface are shown in Figure 5.

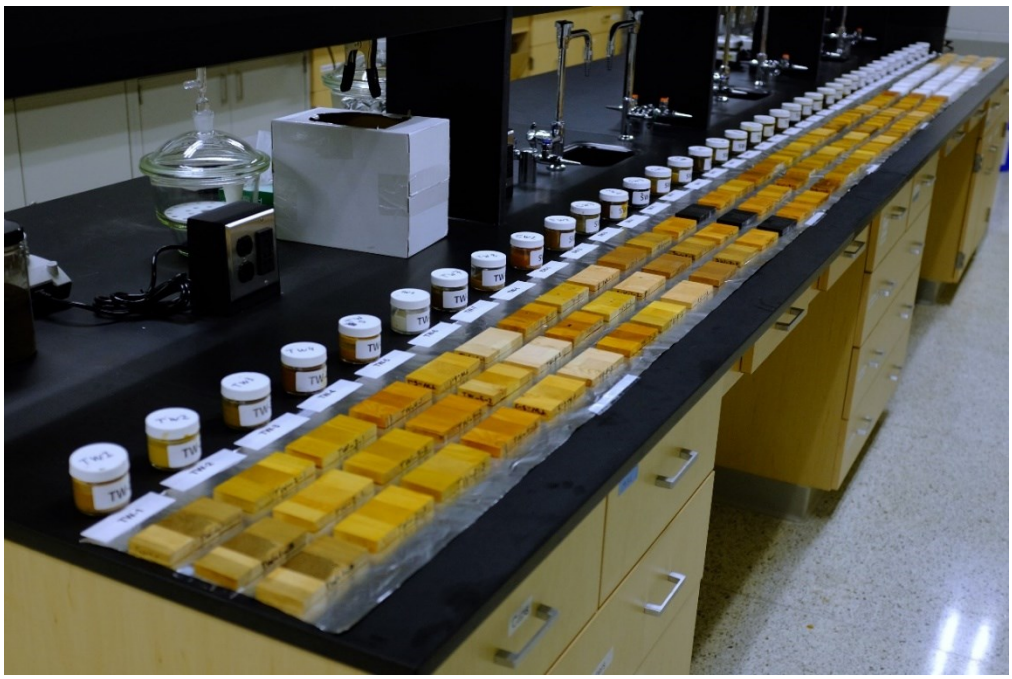

Figure 5. Image of coated small cross-laminated timber (CLT) samples.

All coated and control (uncoated) wood samples were immersed in deionized water at room temperature (22 °C); their weights were measure before and after 2, 4, 8, 24, 48, 72, and 168 h. Each time, wood samples were taken out of the water (one set of 5 replicate samples at a time), and excess surface moisture was removed by a paper towel, the samples were weighed, and then they were immersed in the water again. After 168 h (7 days) of the water immersion test, all wood samples were removed from the water and placed on aluminum foil. Their weights were measured after the same time intervals of air drying to determine the efficacy of each coating on allowing the water vapor to escape from the coated-wood as a measure of water vapor permeability of each coating.

2.7. Data Analysis and Processing

The captured optical images were processed using custom-built code in MATLAB. Data processing was split into two sections: boundary detection and contact angle calculation.

2.7.1. Boundary Detection

To calculate a droplet contact angle, the average droplet diameter must be determined. To achieve this, the edge of the droplet must be distinguished from the wood substrate. Once the

boundary is found, the droplet base area and subsequent average droplet diameter can be determined. In this work, two different boundary techniques were used: Canny detection (water-based coatings) and calibration subtraction (solvent-based coatings).

The traditional boundary detection of droplets and bubbles is achieved using a thresholding technique in a side-view orientation (see Figure 1a) with backlighting [27,38]. Every pixel of a captured image has an associated magnitude. In a grayscale image, the magnitude varies between 0 and 1, with each denoting black and white, respectively. In the case of a side-view orientation (Figure 1a), an LED light behind the bubble or droplet occupies the entirety of the image background, thus giving a uniform field for contrast and simplifying the boundary detection process. Figure 6 shows the optical image processing methodology for the outlined approach. First, the raw image is converted to grayscale (Figure 6a). The image is then binarized using the Otsu method to threshold the image into two sections (Figure 6b). Then the image is filled, and the droplet is isolated by finding the largest area (Figure 6c). Once the droplet shape has been determined, the boundary is traced, and the pixel size is applied to scale the image correctly (Figure 6d).

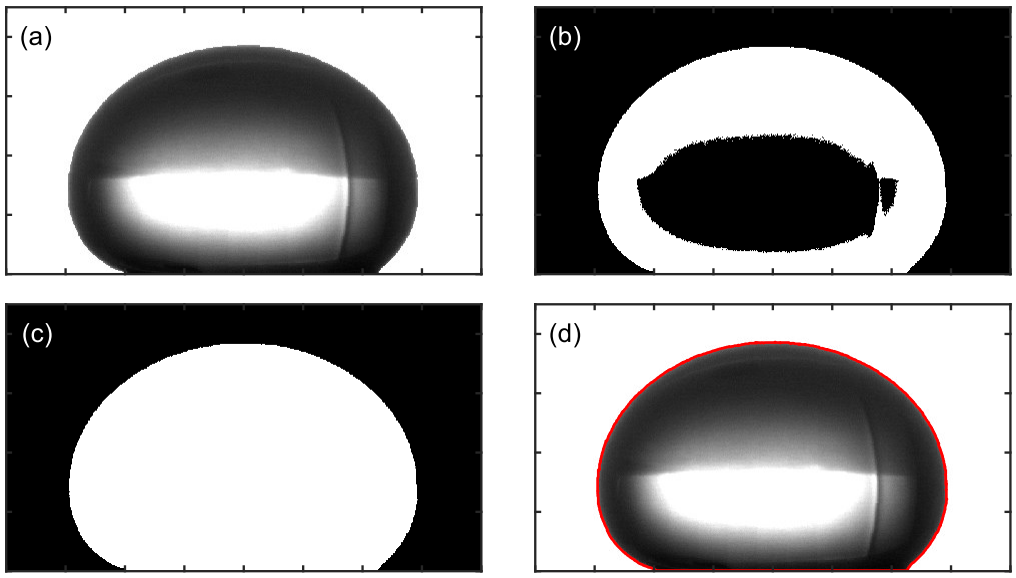

Figure 6. Droplet side-view configuration optical image processing of a superhydrophobic droplet. (**a**) grayscale; (**b**) Otsu threshold; (**c**) binarized and filled; (**d**) boundary traced.

For a coating droplet on a wood surface, the side-view approach is not feasible for two main factors. First, a coating droplet on a wood surface is generally non-axisymmetric due to the anisotropic nature of the substrate, and it typically spreads more along the direction of wood grain than across the grain. Thus, the implementation of a top–down optical configuration is required (see Figure 1b). In this orientation, the wood substrate is the background and the illumination of the imaging area is from above. The sufficient lighting of the droplet and substrate is required to reduce image noise. The combination of the top-down configuration and the natural appearance and texture of the wood substrate can distort the boundary detection between the coating and the wood when using the traditional thresholding technique. The incorrect detection of the droplet boundary can occur when the droplet and the adjacent surface are close in pixel intensity, as shown in Figure 7. Figure 7 shows a coating droplet on a wood substrate at various stages of image processing when using the thresholding approach. First, the raw image is converted to grayscale (Figure 7a). The raw image is binarized using the Otsu method to threshold the image into two sections (Figure 7b). Then, the image is filled, and the droplet is isolated by finding the largest area (Figure 7c). Finally, the boundary is traced and applied over the original image (Figure 7d).

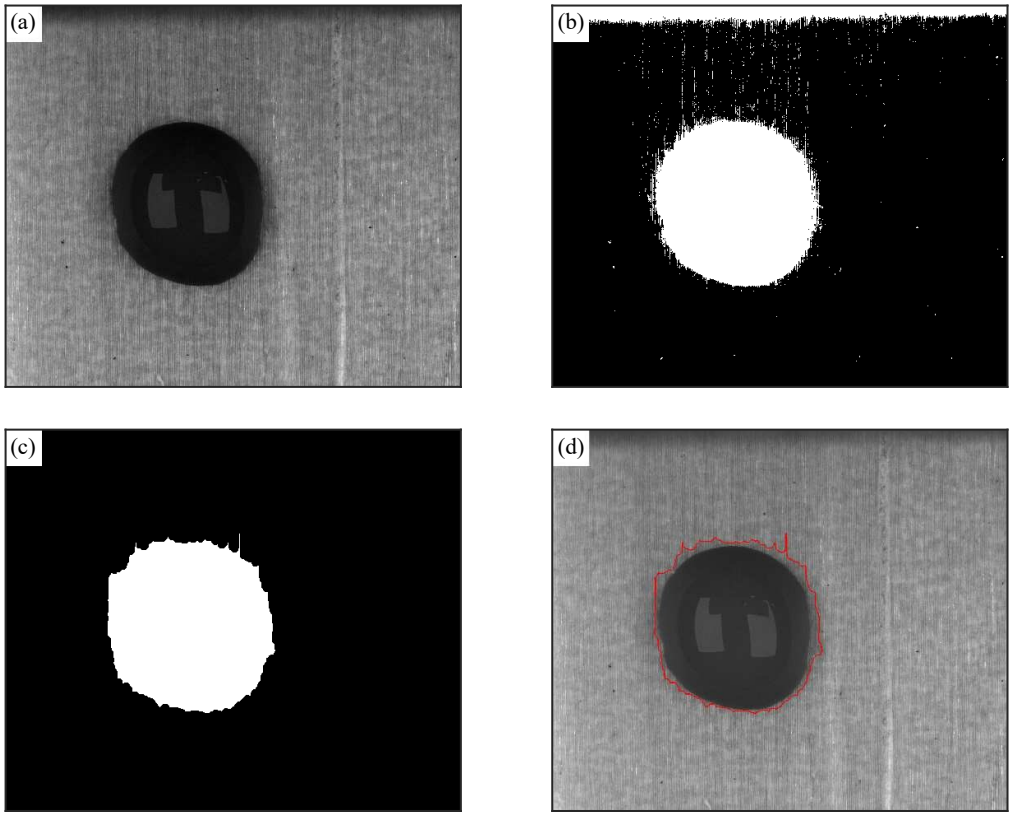

Figure 7. Droplet image processing using the thresholding method at various steps: (**a**) grayscale, (**b**) Otsu threshold, (**c**) filtered, and (**d**) boundary traced.

Wood is a complex, non-homogeneous surface; the natural grain of the woods results in a non-uniform background with the potential to have lighter and darker components than the characterized droplet itself. Due to the similar intensity of the wood grain directly adjacent to the droplet–wood boundary, the initial detection with the Otsu method results in a distorted boundary, resulting in an inaccurate average droplet diameter and, subsequently, calculated contact angle. This case can frequently occur due to the extensive possible combinations of coatings and woods.

In the present work, the Otsu thresholding method was replaced with the Canny edge detection method. The Canny edge detection method characterizes the pixel intensity gradients across an image. For wood, due to its inherent non-homogeneous nature, there are rapidly changing gradients of pixel intensity across the surface, whereas for a droplet of sufficient opaqueness, the pixel field is comparatively uniform. This method utilizes the natural gradients of the wood surface to distinguish it from the droplet. The Canny technique of edge detection is shown in Figure 8 and is the same droplet–wood combination as discussed in Figure 7. Again, the raw image was converted to grayscale (Figure 8a). The image was binarized using the Canny edge detection method to divide the image into two sections (Figure 8b). The image was filtered using morphological closing, the image was then inverted, and then the droplet was isolated by finding the largest area (Figure 8c). The boundary was then traced and applied over the original image (Figure 8d). A droplet with sufficient opaqueness will have minimal gradients, allowing for a clear separation of the wood and droplet using this method. By comparing Figures 7d and Figure 8d, the improved tracking of the droplet boundary when using the proposed method can be seen.

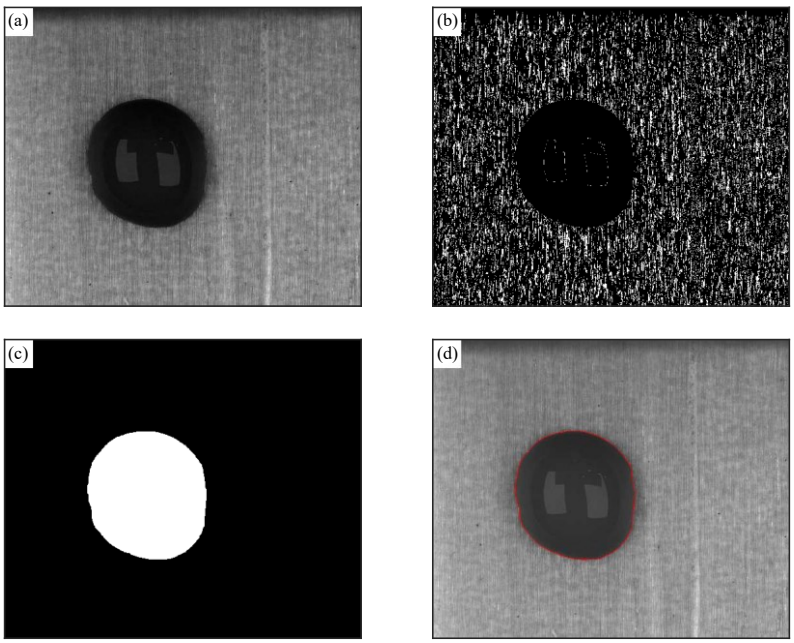

Figure 8. Droplet image processing using the thresholding method at various steps: (**a**) grayscale, (**b**) Canny detection, (**c**) filtered, and (**d**) boundary traced.

A second boundary detection method was required to process the solvent-based coatings characterized in this study. Solvent-based coatings typically spread to a thin transparent layer that disrupts the Canny detection method. An example of the droplet boundary detection using the calibration subtraction method is shown in Figure 9. This approach utilizes an initial set of no drop calibration images that are averaged and then subtracted from the investigated image to distinguish the droplet from the wood background (Figure 9b). A vital component of this technique is to ensure that the camera and the substrate do not change position during droplet placement and data acquisition. The Canny method has the advantage of requiring no set-up in distinguishing the droplet boundary.

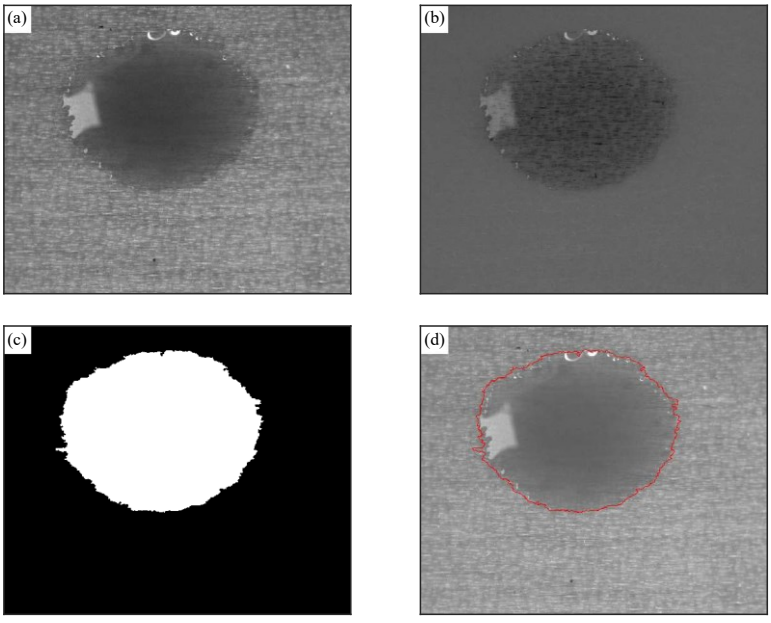

Figure 9. Droplet image processing using the calibration subtraction method at various steps: (**a**) grayscale, (**b**) subtraction, (**c**) filtered, and (**d**) boundary traced.

2.7.2. Contact Angle Calculation

The local mechanical equilibrium between each point of the droplet liquid–gas interface can be expressed by the Young–Laplace equation. For a given volume (V), coating and base diameter (D) only one solution of the Young–Laplace equation exists. Accounting for only hydrostatic effects, this equation is given by [39]:

$$2C = \frac{2\lambda}{r_t} - g(\varrho_l - \varrho_v)(z - z_0), \quad (1)$$

where λ is the measured surface tension of the coating; r_T is the apex radius of the droplet; g is gravity; ρ_l and ρ_v are the density of the coating and ambient air surroundings, respectively; z_0 is the reference height taken as the droplet height; z is the height of the point on the interface being evaluated; and C is the local curvature of the droplet, given by $2C = \frac{1}{r_1} + \frac{1}{r_2}$, where r_1 and r_2 are the principal radii of the droplet at any point on the liquid–gas interface. The initial droplet height and apex radius are estimated as a spherical cap of the same base diameter. Equation (1) evaluates the balance between the pressure difference across the interface and the stress in the interface expressed as the product of the surface tension and the curvature.

Knowing the base diameter and droplet volume, along with working fluid properties such as density and surface tension, one can calculate the droplet shape according to the Young–Laplace equation. Similar to Gibbons et al. [27], an iterative method was employed to calculate the droplet interface profile. The resultant droplet volume of the calculated Young–Laplace curve was compared with that of the experimental data. The tip curvature and height were then adjusted based on this volume ratio, maintaining a fixed base diameter. This process continued until the Young–Laplace solution volume converged to that of the experimental data. A difference of < 0.01 μL was set as the threshold value. An example of the boundary calculated from the Young–Laplace equation is shown in Figure 2a,b. From the calculated boundary, a number of essential parameters such as droplet height (H), contact angle (θ), interfacial areas, and the radii of curvature could be determined. These parameters are shown in Figure 2a,b.

Only one solution of the Young–Laplace equation exists for a given volume and calculated diameter. This method can also be used to solve droplets with $\theta > 90°$. In this case, instead of inputting the base diameter, the maximal diameter of the droplet was used, and the contact angle was calculated in a similar iterative manner as above.

This research was differentiated from previous work by Baptista et al. [33], Erbil et al. [34], and Mchale et al. [35] in its more straightforward application in the real world case and the description of an intelligent boundary detection technique that utilized the natural grain of the wood that also accounted for cases where the coating and wood substrate were similar in color and appearance. The presented technique only requires one camera compared to the three of Baptista et al. and two of Erbil et al. and Mchale et al. The present approach can be employed in cases where comparable droplet geometric lengths and characteristic capillary lengths are observed where gravitational forces dominate over the surface tension effect, such as in solvents with low surface tension properties.

3. Results and Discussion

3.1. Coating Properties

Table 1 shows all the measured coating properties. Overall, there was a strong correlation (r = 0.85) between the pH of coatings and their surface tensions, with water-based coatings having higher pH and surface tension values. Additionally, though not as strong as the pH correlation, higher viscosity coatings also showed higher surface tensions.

Table 1. List of coatings and their measured properties.

No	ID	Producer Name	Trade Name	Type *	Base **	Surface Tension [mN/m]	Solid Content [%]	Viscosity [cP]	pH	T_g (°C)
1	T.S.-1	PPG	Olympic Maximum	T	S	25.7 ± 0.1	37 ± 0.1	72 ± 0.8	6.8 ± 0.12	–18
2	T.S.-2	Cabot	Australian Timber Oil	T	S	26.6 ± 0.1	41 ± 0.3	101 ± 1.2	5.3 ± 0.29	–24
3	T.S.-3	Sherwin Williams	Super Deck	T	S	24.9 ± 0.0	67 ± 0.2	11 ± 0.4	5.7 ± 0.04	–4
4	T.S.-4	Sherwin-Williams	Thompsons Water Seal	T	S	32.0 ± 0.2	73 ± 0.3	372 ± 3.4	5.9 ± 0.06	–8
5	T.S.-5	Akzo-Nobel	Sikkens	T	S	32.6 ± 0.1	73 ± 1.5	74 ± 1	7.8 ± 0.03	–37
6	T.S.-6	Rust-Oleum	Wolman	T	S	26.8 ± 0.1	74 ± 1.4	53 ± 2.5	4.9 ± 0.01	–16
7	S.S.-1	PPG	Olympic	S	S	26.4 ± 0.2	36 ± 0.3	7 ± 0.1	4.5 ± 0.01	–19
8	S.S.-2	Gemini	TWP	S	S	26.1 ± 0.0	37 ± 0.2	14 ± 0.3	5.3 ± 0.06	–12
9	S.S.-3	Sherwin Williams	Super deck	S	S	26.0 ± 0.1	70 ± 0.7	29 ± 1	4.6 ± 0.01	–38
10	S.S.-4	Sherwin Williams	Duckback	S	S	30.4 ± 0.3	79 ± 0.7	92 ± 0.6	4.0 ± 0.03	–13
11	T.W.-1	PPG	Flood	T	W	37.5 ± 0.4	27 ± 1.0	1390 ± 4	7.1 ± 0.01	–19
12	T.W.-2	Benjamin Moore	Arborcoat	T	W	43.4 ± 0.8	30 ± 0.1	490 ± 2	8.7 ± 0.03	6
13	T.W.-3	Behr	Weatherproofing	T	W	44.9 ± 0.9	28 ± 0.2	500 ± 3	9.4 ± 0.01	–18
14	T.W.-4	Behr	Weatherproofing	T	W	44.1 ± 1.0	28 ± 0.2	830 ± 2	9.4 ± 0.02	–17
15	T.W.-5	PPG	Flood-CWF-UV-5	T	W	35.4 ± 0.3	30 ± 1.1	760 ± 4	7.3 ± 0.01	–11
16	S.W.-1	Rust-Oleum	Wolman	S	W	46.2 ± 0.4	14 ± 1.0	560 ± 5	9.2 ± 0.01	–7
17	S.W.-2	Sherwin Williams	Super deck	S	W	60.8 ± 0.1	40 ± 0.2	1845±21	9.4 ± 0.01	–11
18	S.W.-3	Benjamin Moore	Arborcoat	S	W	42.1 ± 0.5	25 ± 1.7	400 ± 3	8.9 ± 0.01	6
19	S.W.-4	PPG	Olympic Maximum	S	W	34.3 ± 0.1	17 ± 0.4	450 ± 2	8.7 ± 0.02	–12
20	S.W.-5	PPG	Flood	S	W	39.3 ± 0.1	32 ± 0.2	457 ± 2	9.0 ± 0.01	–12
21	P.W.-1	PPG	Speed Cryl	P	W	54.1 ± 0.6	49 ± 0.2	9240 ± 6	9.2 ± 0.01	15
22	P.W.-2	Sherwin Williams	Emerald	P	W	49.5 ± 0.4	59 ± 0.2	9250 ± 6	9.8 ± 0.02	–19
23	P.W.-3	Behr	Wood stain	P	W	41.6 ± 0.4	53 ± 0.6	795 ± 3	7.9 ± 0.01	5

Note: * Type (T = transparent; S = semitransparent; and P = paint) and **Base (S = solvent; W = water).

3.2. Contact Angel Data

Figure 10 shows the contact angle evolution with time of spreading S.W.-1 droplets on wood substrates for both early and latewood cases. In both wood type cases, the contact angle of the S.W.-1 droplet initially decreased before reaching a minimum contact angle between t = 1–1.5 min. After that, the contact angle leveled off with a marginal increase as the droplets achieved equilibrium and began to solidify in ambient conditions. This trend was typical for all test cases. The experimental uncertainty for all parameters was examined using the methodology outlined by Kirkup and Frenkel [40] to a 95% confidence level. An average percentage uncertainty of 18% was calculated for all contact angle measurements. This was determined by applying a combined uncertainty approach to Equation (1), accounting for the uncertainty in measuring the droplet diameter, surface tension, and volume. Figures 11–13 incorporate error bars to highlight the individual uncertainty associated with each coating measurement.

Figure 11 plots the average contact angle for the solvent-based coatings for both early and latewood cases at t = 1 min. Coatings are divided into the semi-transparent stain (Figure 11a) and transparent stain (Figure 11b). In general, a larger contact angle was observed on latewood in comparison to earlywood, and this was consistent with results previously published in the literature [20].

It should be noted that the difference between the average contact angles of early and latewood cases were within the calculated experimental uncertainty.

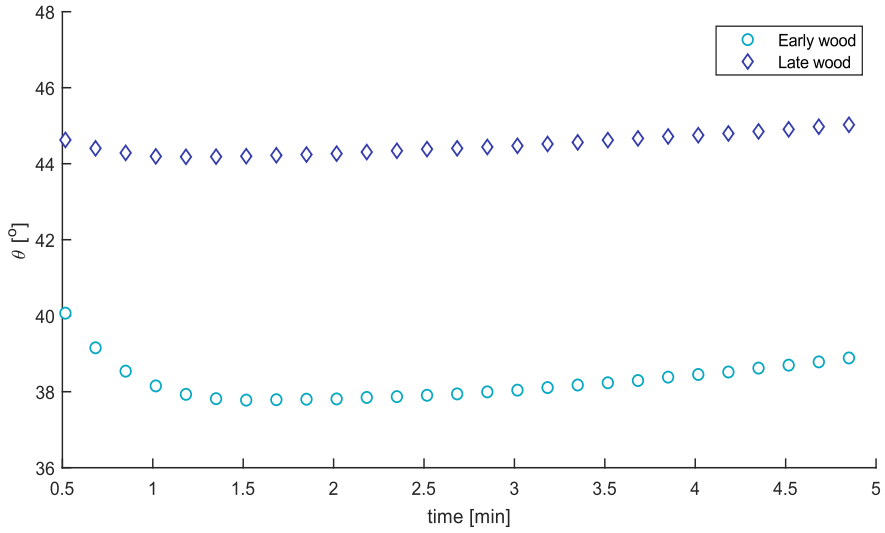

Figure 10. Time evolution of S.W.-1 coating contact angle of on wood substrate.

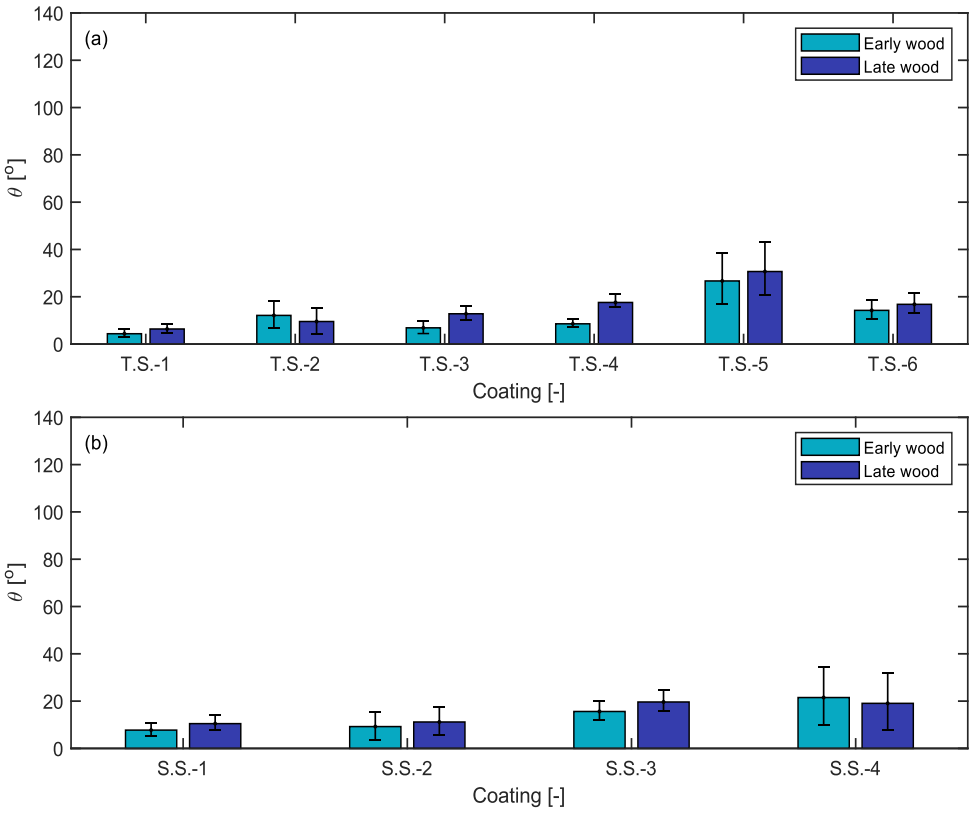

Figure 11. Average coating contact angle at t = 1 min: (**a**) S.S. (semi-transparent stain, solvent-based) and (**b**) T.S. (transparent stain, solvent-based).

Figure 12 plots the average contact angle of the water-based coatings for both early and latewood cases at t = 1 min. Coatings are divided by their base constitution and density of their pigmentation: semi-transparent stain (Figure 12a), paint (Figure 12b), and transparent stain (Figure 12c). In agreement with previous literature and the solvent-based coatings, a larger contact angle was generally observed for latewood than earlywood.

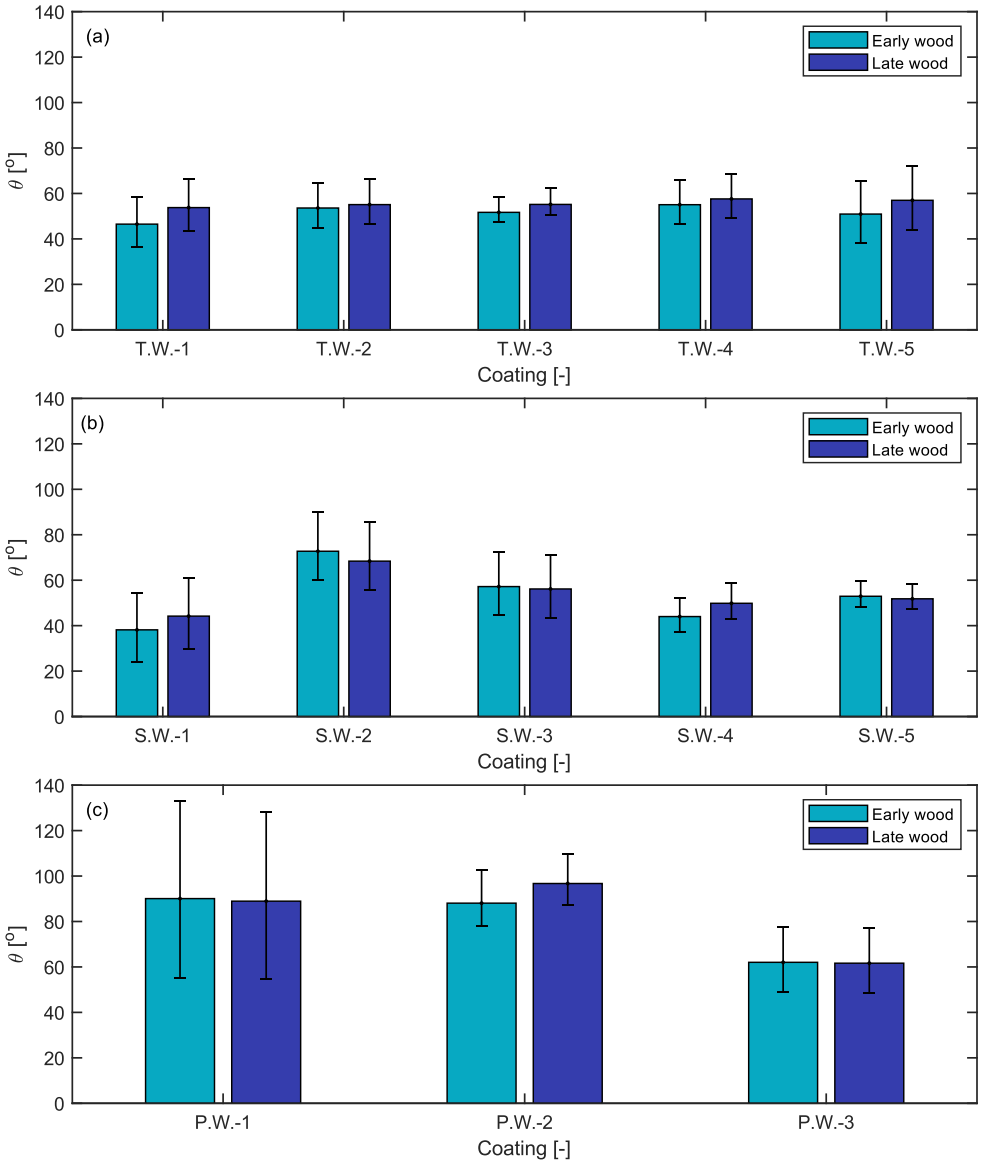

Figure 12. Average coating contact angle at t = 1 min: (**a**) S.W. (semi-transparent stain, water-based), (**b**) P.W. (paint, water-based), and (**c**) T.W. (transparent stain, water-based).

Figure 13 compares the average contact angle of the water and solvent coatings for early and latewood cases. The largest average contact angles were observed for the water-based paints (P.W.) of 80° and 82° for the early and latewoods, respectively. The smallest contact angles were observed in the transparent solvent-based stain coating of 12° and 15° for the early and latewoods, respectively. By comparing the coating across their base structure, it can be noted that the solvent-based coatings had a significantly lower contact angle than their water-based counterparts. This trend is further explored in Figure 14.

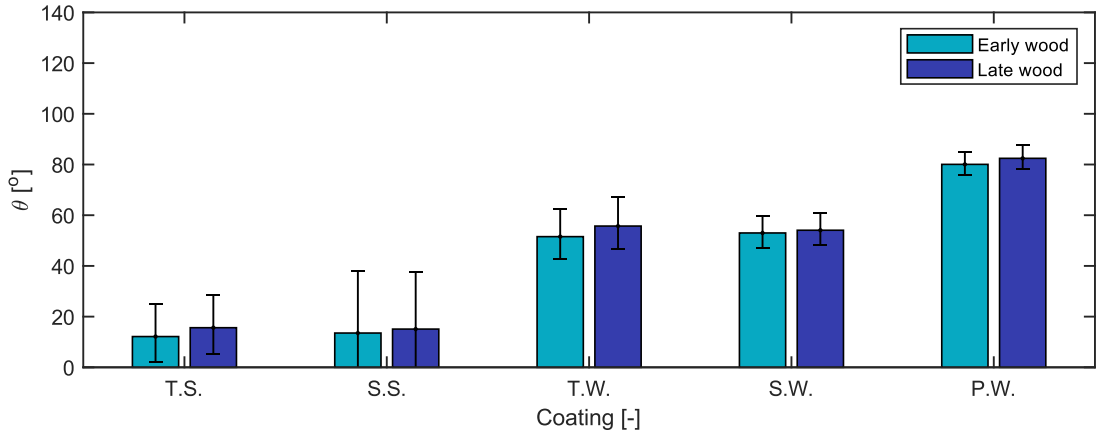

Figure 13. Average coating contact angle for all coatings at t = 1 min.

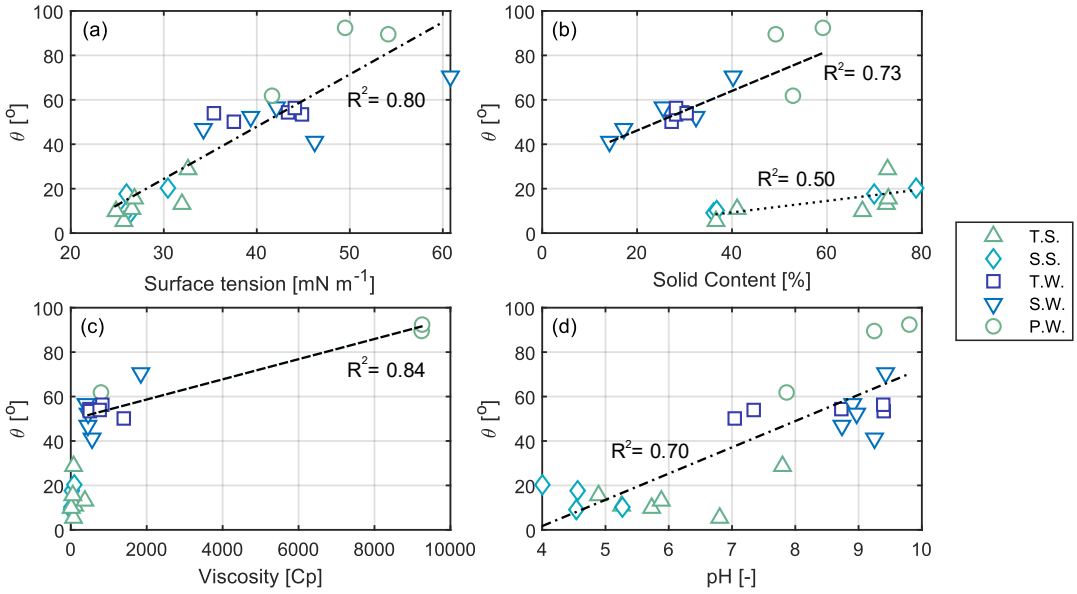

Figure 14. Contact angle dependency on various fluid properties: (**a**) surface tension, (**b**) solid content, (**c**) viscosity, and (**d**) pH. Dashed lines (---) are water-based coating trends, dotted lines (···) are for solvent-based coatings, and alternating dash–dot lines (· — ·) are for combined water and solvent-based trends.

Figure 14 compares four coating properties with the average measured contact angle of the early and latewood cases. This approach was taken to investigate the pertinent fluid properties in coating wetting. Four properties were investigated; surface tension (Figure 14a), solid content (Figure 14b), viscosity (Figure 14c), and pH (Figure 14d). From the data, it can be noted that there was a strong correlation between the measured contact angle and surface tension (89%) and pH (84%) for all coatings (Figure 14a,d). The correlation of pH and contact angle can be attributed to the strong correlation of pH with the type of coatings (water or solvent-based). When the coatings were split by their solvent or water bases, 86% and 71% correlations were noted for contact angle and solid content (Figure 14b) for the water and solvent-based coatings, respectively. A 92% correlation was observed for the water-based coatings for contact angle and coating viscosity (Figure 14c). It is important to note that for the highest viscosities, a coating may take longer than the measurement period to reach equilibrium.

A lower contact angle indicates better wetting and subsequent greater bond strength and coating performance [26]. Focusing on the semi-transparent penetrating stains, the results showed that the average surface tensions (44 mN/m) of the water-based formulations (five different coatings) were 61% higher than their solvent-based counterparts (27 mN/m, four different coatings). In 2016, we also measured the properties of 14 commercially available exterior wood coatings in the North American

market [26]. The average surface tension of those coatings showed that water-based formulations had, on average, much higher surface tension (32 mN/m) than solvent-based coatings (25 mN/m). The optimization of water-based coating formulations has stagnated. Ideally, a formulated coating should have a significantly lower surface energy than that of the substrate to which it is applied [23]. In a previous study [41], the present authors demonstrated that the addition of 0.1% of additives such as defoamers (Surfynol MD20), surfactants (BYK-346, Twin 4100, and Dynol 960), and wetting agents (Hydropalat WE3322) could significantly reduce the surface tension of a water-based polyurethane resin from 44 to 20–29 mN/m. These results, in tandem with the data presented in Figure 15, showed that coating formulators should incorporate proper additives to reduce the surface tension of water-based formulation and increase coating wetting and adhesion, thus extending their lifecycle.

3.3. Water Immersion Testing

Figure 15 shows the moisture content changes of coated and uncoated wood samples after 2, 4, 8, 24, 72, and 168 h of water immersion and the same interval after placing at room temperature for air drying. All coatings showed a sharp increase in moisture content during the initial submersion period (t = 0–8 h), with a general increase observed until the samples were unsubmerged at t = 168 h (7 days). After that (t = 168–336 h), a decrease in the moisture content was noted for all samples, with a decreasing rate of drying as the samples approach steady-state conditions. Sensibly, the most significant moisture content change was noted for the uncoated sample. A higher moisture uptake was seen for the water-based coatings in comparison with their solvent-based counterparts. Interestingly, the maximum achieved moisture content was observed to be proportional to the contact angle data discussed in Figure 15. The largest moisture content uptake was noted for the water-based paint coating, which had the largest average contact angle of 81°. In contrast, the smallest moisture content at t = 168 h was calculated for the transparent stain coating, which had the smallest average contact angle of 13.9°. Similar trends were noted for the drying section of the test, with the water-based paint coating moisture content decreasing at the most rapid rate and the solvent-based coatings drying slower than their water-based counterparts. Overall, all coated samples had significantly lower water uptakes than uncoated wood samples and an reached equilibrium moisture content (MC of around 5%) after 72 h of air drying, similar to uncoated wood samples, thus indicating an excellent water vapor permeability.

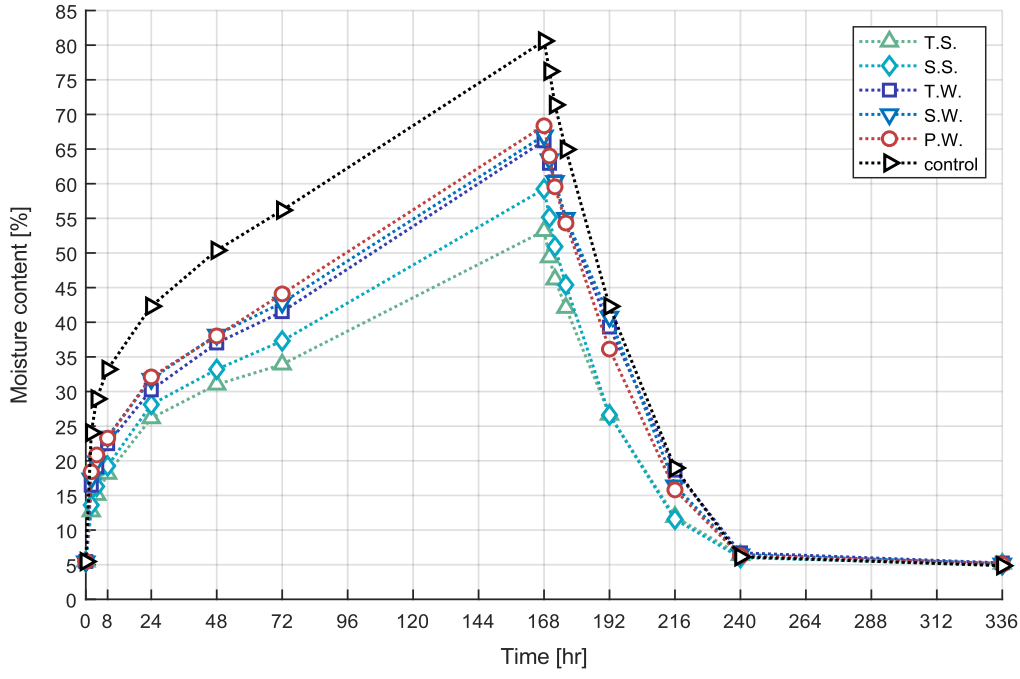

Figure 15. Moisture content changes in coated and uncoated wood samples after 168 h (7 days) of water immersion and then after 7 days of air-drying indication water permeability of samples.

Figure 16 shows the average moisture content changes of all coated samples after 2 and 168 h (7 days). Overall, the solvent-based coatings had much a lower water uptake than the water-based coatings. Surprisingly, transparent coatings, both water-based and solvent-based, had, on average, a lower water uptake (higher moisture resistance) than the semi-transparent and paint samples. Though this was a lab test, it is a representation of how these coatings would perform when exposed to long term natural weathering in service. It is interesting to observe that solvent-based coatings available in the North American market for exterior wood coatings outperformed water-based coatings, possessing lower surface tension, lower contact angles, and better water resistance. In ongoing research work by the present authors, the best six performing coatings (based on measured coating properties and lab performance) in this study have been selected to evaluate their efficacy in protecting cross-laminated timber (CLT) samples over five years of natural weathering in two sites in the United State (Mississippi and Wisconsin).

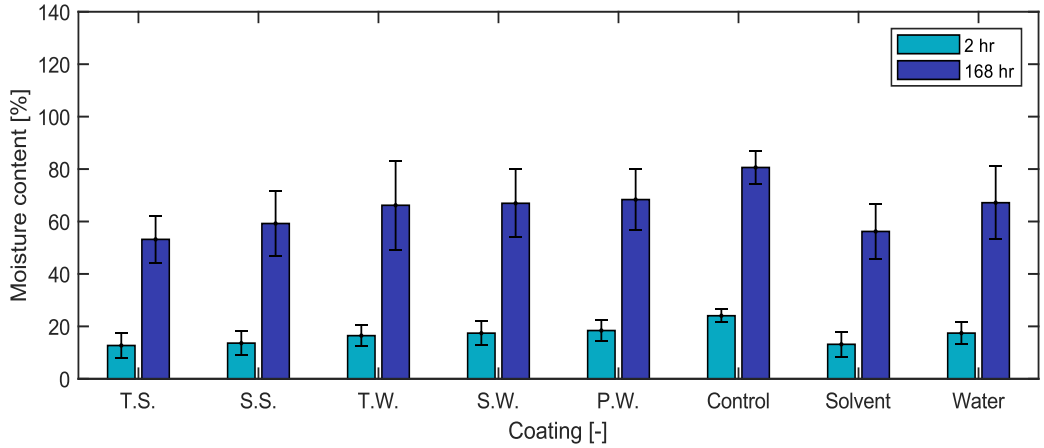

Figure 16. Moisture content changes in coated and uncoated wood samples after 2 and 168 h (7 days) of water immersion.

4. Conclusions

The properties of thirteen water-based and ten solvent-based coatings, including their temporal wetting, were investigated. Across all characterized coatings, an 11% larger average contact angle was noted for latewood compared to earlywood. This was due to the higher density of latewood compared with earlywood in general, but it is more pronounced in southern yellow pine.

Investigating the relationship between the measured contact angle and a selection of coating properties revealed a strong correlation between the coating contact angle with surface tension and the pH of the coatings. When the coatings were split by their solvent and water bases, an increase in the solid content was also shown to increase the contact angle. In contrast, a 92% correlation was observed with the contact angle and viscosity of the water-based formulations.

The average contact angle (60°) and surface tension (44 mN/m) of the water-based formulations were significantly higher than that of their solvent-based counterparts (14°, 28 mN/m). The greater wetting of the solvent coatings in comparison to their water counterparts was due to the organic solvent, which inherently resulted in a reduced surface tension property. Additionally, 73% and 74% decreases in the measure contact angle were noted for the solvent-based coatings when comparing the semi-transparent stain and transparent stain with their water-based counterparts, respectively. These results suggested that surface tension could provide a good prediction for coating spreading.

To increase the application of water-based coatings and improve their performance, it is crucial to reduce their surface tension and thus their contact angle, which would enhance coating performance. A new innovative technique for characterizing the wetting properties of coating droplets on wood surfaces was also demonstrated. The automated calculation of the coating contact angle, which is a direct predictor of coating bond strength, was shown when utilizing the wood grain in determining the droplet–wood boundary. This methodology can be applied to an industrial setting

to improve coating adhesion performance, reduce maintenance, and extend the service of coated wood products.

Water-based coatings demonstrated a higher average water uptake compared with their solvent-based counterparts. Conversely, they also showed a higher water-vapor permeability, enabling water-based coated-wood samples to let absorbed water evaporate at a faster rate than solvent-based coated wood samples. It should be noted that the water uptake testing was lab-based, and ongoing natural weathering testing will enable further insights into these results. To increase the widespread use of water-based coatings, it is crucial to improve their wettability by reducing their surface tension. This can be achieved by augmenting coating formulations using suitable additives.

Author Contributions: This study was convinced and designed by M.N.; experiments were conducted by S.N., T.S., and K.O.; Results and data were analyzed by M.J.G., T.S. and S.N.; approved by M.N., S.C.; the first draft was written by M.J.G. All authors reviewed and revised the manuscript to produce the final version.

Funding: This research was funded by USDA Forest Products Laboratory, 16-JV-11111136-048 and supported by the USDA National Institute of Food and Agriculture, McIntire Stennis, 1021850.

Acknowledgments: The authors would like to thank Maryam Arefmanesh for her help with surface tension analysis and the United States Department of Agriculture, Forest Product Laboratory (Madison) for funding support.

Conflicts of Interest: The authors declare no conflict of interest.

Nomenclature

C	Curvature [m^{-1}]
D	Droplet average diameter [m]
g	Gravitational acceleration [$m\ s^{-2}$]
H	Droplet height [m]
r	Radius [m]
S	Coordinate [mm]
t	Time [min]
V	Droplet volume [μL]
z	Local height of the liquid–gas interface [m]
Subscript	
t	Apex
Greek Symbol	
λ	Surface tension [$N\ m^{-1}$]
θ	Contact angle [°]
Acronyms	
S.W.	Semi-transparent stain, water-based
P.W.	Paint, water-based
T.W.	Transparent stain, water-based
S.S.	Semi-transparent stain, solvent-based
T.S.	Transparent stain, solvent-based

References

1. Wilson, J.D.; Hamilton, J.K. Wood cellulose as a chemical feedstock for the cellulose esters industry. *J. Chem. Educ.* **1986**, *63*, 49.
2. Janes, R.L. *The chemistry of wood and fibers.* 2nd ed.; McGraw-Hill Book Company: New York, NY, USA, 1969.
3. Carraher, C.E.; Seymour, R.B. Polymer structure-organic aspects (definitions). *J. Chem. Educ*. **1988**, *65*, 314.
4. Britt, K.W. *Handbook of pulp and paper technology*. 2nd ed.; Reinhold Publishing Corp.: New York, NY, USA, 1970.
5. Schaller, C.; Rogez, D. New approaches in wood coating stabilization. *J. Coat. Technol. Res.* **2007**, *4*, 401–409.

6. Nejad, M.; Cooper P. Exterior wood coatings. In *Wood in Civil Engineering;* Concu, G. Ed.; Intech: Rijeka, Croaita, 2017; pp. 111–129.
7. Nejad, M.; Shafaghi, R.; Pershin, L.; Mostaghimi, J. Cooper P. Thermal spray coating: A new way of protecting wood. *BioResources* **2017**, *12*, 143–156.
8. Feist, W.C. Exterior wood finishes. *Coat. Technol. Handb*. **2006**, *111*, 1–12.
9. Feist, W.C.; Hon, D.N. Chemistry of weathering and protection. In *The Chemistry of Solid Wood;* Rowell1, R., Ed.; ACS Publications: Washington, DC, USA, 1984.
10. Hon, D.N.; Shiraishi, N. *Wood and Cellulosic Chemistry, Revised, and Expanded*, 2nd ed.; CRC press: Boca Raton, FL, USA, 2000.
11. Agarwal, U.P.; Atalla, R.H. Raman Spectroscopic Evidence for Coniferyl Alcohol Structures in Bleached and Sulfonated Mechanical Pulps. In *Photochemistry of Lignocellulosic Materials*; Rowell1, R., Ed.; ACS Publications: Washington, DC, USA, 1993.
12. Schniewind, A.P. Mechanism of check formation. *For. Prod. J.* **1963**, *13*, 475–480.
13. Simpson, W.; TenWolde, A. *Physical Properties and Moisture Relations of Wood*; The United States Department of Agriculture: Washington, DC, USA, 1999.
14. Edward, J.O.D. Structural Integrity and Physical Properties of Ponderosa Pine over Time after Death between Vectors of Mortality. Master's Thesis, University of Montana, Missoula, MT, USA, 2017.
15. Service, F.; Feist, W.C.; Little, J.K.; Wennesheimer, J.M. *The Moisture-Excluding Effectiveness of Finishes on Wood Surfaces*; US Department of Agriculture, Forest Service, Forest Products Laboratory: Wisconsin, WI, USA, 1985.
16. Brito, V.; Gonçalves, T.D.; Faria, P. Coatings applied on damp building substrates: performance and influence on moisture transport. *J. Coat. Technol. Res*. **2011**, *8*, 513–525.
17. Feist W.C. Weathering and protection of wood. In Proceedings of seventy-ninth annual meeting of the American Wood-Preservers' Association, Kansas City, MI, USA, 17–20 April 1983.
18. Ekstedt, J.; Östberg, G.; Liquid water permeability of exterior wood coatings-testing according to a proposed European standard method. *J. Coat. Technol.* **2001**, *73*, 53–59.
19. Dickie, R.A. Toward a unified strategy of service life prediction, *J. Coat. Technol*. **1992**, *64*, 61–64.
20. Williams, R.S.; Jourdain, C.; Daisey, G.I.; Springate, R.W. Wood properties affecting finish service life. *J. Coat. Technol.* **2000**, *72*, 35–42.
21. Feist, W.C. Wood properties and finish durability, *J. Coat. Technol.* **2002**, *74*, 71–76.
22. Jourdain, C.; Dwyer, J.; Kersell, K.; Mall, D.; McClelland, K.; Springate, R.; Williams, S. Changing nature of wood products—What does it mean for coatings and finish performance? *J. Coat. Technol*. **1999**, *71*, 61–66.
23. Weldon, D.G. *Failure Analysis of Paints and Coatings*; John Wiley & Sons: Hoboken, NJ, USA, 2009.
24. Kazayawoko, M.; Neumann, A.W.; Balatinecz, J.J. Estimating the wettability of wood by the Axisymmetric Drop Shape Analysis-contact Diameter method. *Wood Sci. Technol*. **1997**, *31*, 87–95.
25. Packham, D.E. *In Handbook of Adhesion Second Edition*, 2nd ed.; John Wiley & Sons: West Sussex, UK, 2005.
26. Nejad, M.; Cooper, P. Exterior wood coatings. Part-2: modeling correlation between coating properties and their weathering performance. *J. Coat. Technol. Res.* **2011**, *8*, 459–467.
27. Gibbons, M.J.; Di Marco, P.; Robinson, A.J. Local heat transfer to an evaporating superhydrophobic droplet. *Int. J. Heat Mass Transf.* **2018,** *121*, 641–652.
28. Gibbons, M.J.; Di Marco, P.; Robinson, A.J. Heat flux distribution beneath evaporating hydrophilic and superhydrophobic droplets. *Int. J. Heat Mass Transf*. **2020**, *148*, 119093.
29. Jordan, D.L.; Wellons, J.D. Wettability of dipterocarp veneers. *Wood Sci.* **1977**, *10*, 22–27.
30. Nguyen, T.; Johns, W.E.; Polar and dispersion force contributions to the total surface free energy of wood, *Wood Sci. Technol.* **1978**, *12*, 63–74.
31. Shi, S.Q.; Gardner, D.J. Dynamic adhesive wettability of wood, *Wood Fiber Sci.* **2001,** *33*, 58–68.
32. De Meijer, M.; Haemers, S.; Cobben, W.; Militz, H. Surface energy determinations of wood: Comparison of methods and wood species. *Langmuir* **2000**, *16*, 9352–9359.
33. Baptista, D.; Muszyński, L.; Gardner, D.J.; Atzema, E. An experimental method for three-dimensional dynamic contact angle analysis. *J. Adhes. Sci. Technol.* **2012**, *26*, 2199–2215.
34. Erbil, H.Y.; Meric, R.A. Evaporation of sessile drops on polymer surfaces: Ellipsoidal cap geometry, *J. Phys. Chem. B* **1997**, *101*, 6867–6873.
35. McHale, G.; Erbil, H.Y.; Newton, M.I.; Natterer, S. Analysis of shape distortions in sessile drops. *Langmuir* **2001**, *17*, 6995–6998.

36. *STM D2369-01 Standard Test Method for Volatile Content of Coatings*; ASTM International: West Conshohocken, PA, USA, 2001.
37. *ASTM D3418-15, Standard Test Method for Transition Temperatures and Enthalpies of Fusion and Crystallization of Polymers by Differential Scanning Calorimetry*; ASTM International: West Conshohocken, PA, USA, 2015.
38. Donoghue, D.B.; Albadawi, A.; Delaure, Y.M.C.; Robinson, A.J.; Murray, D.B. Bubble impingement and the mechanisms of heat transfer. *Int. J. Heat Mass Transf.* **2014**, *71*, 439–450.
39. Siedel, S.; Cioulachtjian, S.; Robinson, A.J.; Bonjour, J. Integral momentum balance on a growing bubble. *Phys. Fluids.* **2013**, *25*, 123301.
40. Kirkup, L.; Frenkel, R.B. *An Introduction to Uncertainty in Measurement: using the GUM (Guide to the Expression of Uncertainty in Measurement)*; Cambridge University Press: Cambridge, UK, 2006.
41. Nejad, M.; Arefmanesh, M.; Henderson, K.; Esmaeelpanah, J.; Chandra, S.; Mostaghimi, J. Waterborne Coating Caught on Camera. *Eur. Coat. J.* **2015**, *10*, 30–34.